Journal of Spectroscopy and Molecular Sciences

Journal Homepage: https://dergipark.org.tr/tr/pub/jsms

Ab-initio study of structural, spectroscopic, and electronic properties of (E)-1-(4-Methoxyanthracen-1-yl)-2-phenyldiazene azo dye molecule

Arini Qurrata Ayun[1,*], Pınar Tunay Taşlı[1], Sevgi Ozdemir Kart[1,*]

[1]Pamukkale University, Art & Science Faculty, Physics Department, Denizli, Türkiye

*Correspondence: ariniqurrataayun0@gmail.com (Arini Qurrata Ayun), ozsev@pau.edu.tr (Sevgi Ozdemir Kart)

ORCIDs Arini Qurrata Ayun: https://orcid.org/0000-0002-4739-0507
Pınar Tunay Taşlı: https://orcid.org/0000-0001-6580-9765
Sevgi Ozdemir Kart: https://orcid.org/0000-0001-5706-7722

Abstract: (E)-1-(4-Methoxyanthracen-1-yl)-2-phenyldiazene or $C_{21}H_{16}N_2O$ is one of the tautomer azo dye molecules which is the most usable compound in several industries as a sensing molecule, nowadays. As we know, more than 90% of the existing commercial azo dye is tautomeric ones (Kelemen, 1981). The computational quantum chemistry methods can clarify the relationship between structures and electrochemical properties of molecular compounds for future applications. In this study, the main purpose is to characterize the structural geometries of the title molecule ((E)-1-(4-Methoxyanthracen-1-yl)-2-phenyldiazene), spectroscopic and electronic properties by utilizing ab-initio method based on Density Functional Theory (DFT) (Becke, 1988; Becke, 1993). The molecular geometry and vibrational modes, in the ground state, have been computed by applying DFT/B3LYP method with the basis set of 6-311G (d,p). The structural properties, such as bond length, bond angle, and dihedral angle, are in excellent agreement with those of available experiment data (Crochet et al., 2011). 114 vibrational modes have been specified with stretching, in-plane-bending, out-of-plane-bending, and torsion vibrations (Scott and Radon, 1996). UV-Vis absorption spectrum within dimethyl sulfoxide (DMSO) solvent has been predicted by using Time-Dependent Density Functional Theory (TD-DFT) (Ronca et al., 2014). Moreover, ^{1}H and ^{13}C-NMR chemical shifts have been computed in DMSO solvent by using the Gauge-Invariant Atomic Orbital (GIAO) approach within DFT/B3LYP method (Wolinskiet et al., 1998). Finally, the electronic properties of the title molecule have been also attained by using Koopman's Theorem enable to determine the Lowest Unoccupied Molecular Orbital - Highest Occupied Molecular Orbital (HOMO-LUMO) interaction (Sastri and Perumareddi, 1997). It can be reported that this molecule has gap energy (Eg) bigger than 1.5 eV which indicates thermodynamically stable and durable, low ionization potential energy (IP) which tends to be reducing agents because it is easily losing its electron, about 2.43 eV electron affinity (EA) which denotes that it has good conductive properties, high electronegativity (x) which shows that the title molecule is a polar character, low value of chemical hardness (η) and global electrophilicity index.

Keywords: DFT; UV absorption; chemical shifts; electronic properties; azo dye.

1. Introduction

The development of technology is growing rapidly day by day. Hence, the importance of fast data transmission and processing also become indispensable for nowadays society (Kelemen, 1981). Accordingly, ultrafast, smaller, environmentally friendly, and switchable components

Received 15 June 2022, Accepted 14 November 2022, Available online 25 December 2022.
This work has been presented in TURCMOS2022.

become more important. Azo dye is an organic compound that contains a conjugated in a combined diazotize together with one more azo bond ($-N=N-$) (Benkhaya et al., 2020; Tunay Taslı et al., 2020). One of the important kinds of azo dye is tautomers that generally differ only in the number of electrons and protons when only a transfer of proton reaction occurs between these compounds (Habibi et al., 2006; Shawali et al., 2002). The tautomerism, in azo dyes, is used for the development of certain characteristics such as light fastness, dye tinctorial power, etc (Alsantali et al., 2022; Bayer et al., 1976; Chen et al., 2012; Huang et al., 2022; Lee et al., 2010). Nowadays, more than 90% of the existing commercial azo dye is in a tautomeric form which makes the investigation of their characteristics growing popular. Especially, the structures and characteristics of azo dye have been interested in the applications of switching molecules (Benkhaya et al., 2020; Coelho et al., 2012).

Experimentally, (E)-1-(4-Methoxyanthracen-1-yl)-2-phenyldiazene has been synthesized and its crystal structures, such as bond lengths, bond angles and dihedral angles, have been estimated by using full covariance matrix by Crochet et al. (2011). However, its spectroscopic and electronic properties have not been cleared yet. A comparison of the experimental and theoretical calculations can be very useful in making correct assignments and understanding the relationship between molecular structures and their properties. Therefore, the purpose of this study is to characterize the title molecule, (E)-1-(4-Methoxyanthracen-1-yl)-2-phenyldiazene, by utilizing the computational quantum chemistry methods to understand its chemical and physical properties at the atomistic level, and the to identify the electronic properties of the title molecule.

The computational quantum chemistry methods are very powerful tools to determine and analyze the structural properties of chemical molecules. The interest in this method is increasing progressively in recent years, because of their efficiency and low cost with great accuracy. This method simplifies the many-body electron problems by adding quantum interactions (Lee and Yang, 1959). Recently, much interest has been devoted to clarify the physical and chemical properties of different azo dye molecules. Tunay Tasli et al. (2020) have obtained the structural and vibrational properties of newly synthesized azo dye material by using the ab-initio method based on the Density Functional Theory (DFT). Yıldırım et al. (2021) have investigated some spectroscopic properties of Amino-pyrazoles by the computational study. Karabacak Atay et al. (2019) have studied the structural characterization and absorption properties of newly synthesized mono azo dye both experimentally and theoretically by using DFT. All these studies have shown that the structural and spectroscopic properties of azo dye molecules have been obtained successfully by the computational quantum chemistry method.

In this point of view, the structural properties of the title molecule interested in this study, such as the bond lengths, bond angles and dihedral angles, have been calculated by using DFT method with the basis set B3LYP/6-311G (d,p) in the ground state (Kohn and Sham, 1965; Becke, 1993). To investigate the compatibility between the calculational and experimental results of the bond lengths, bond angles and dihedral angles from the optimized geometries have been compared by using linear regression analysis (Cameron and Windemeijer, 1995). For further characterization of the title molecule, FT-IR, UV-Vis, ^{1}H-NMR and ^{13}C-NMR spectroscopic properties as well as some electronic properties have been revealed by utilizing the ab-initio simulation method based on DFT. To the best of our knowledge, this work presents the theoretical characterization of the title molecule.

2. Materials and methods

2.1. Materials

The structural, spectroscopic, and electronical properties of the title molecule ((E)-1-(4-Methoxyanthracen-1-yl)-2-phenyldiazene) synthesized by Crochet et al. (2011) are clarified by using the computational quantum chemistry methods. The schematic view of the title molecule experimentally by Crochet et al. (2011) as well as the optimized structure of the title molecule via GaussView 5.0 (Frisch, 2016) are shown in the Figure 1.

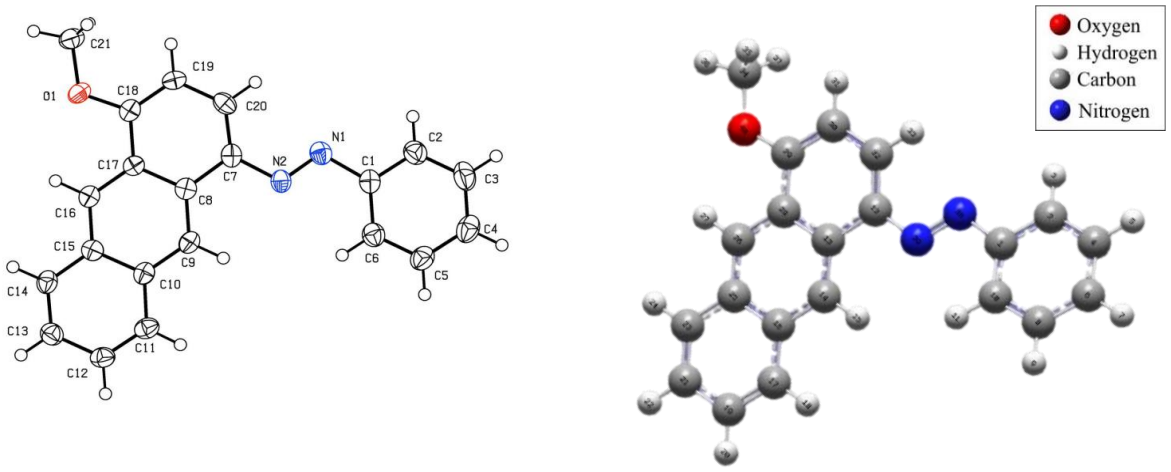

(a) **(b)**

Figure 1. (a) The schematic view of the title molecule synthesized by Crochet et al. (2011) and **(b)** the optimized structures of the title molecule via GaussView 5.0.

2.2. Computational method

This research is based on the ab-initio method, which is a computational method without needing any empirical data about the molecular system of the title molecule. Theoretical studies are carried out by the Gaussian 09W (Frisch, 2016) package program based on the computational quantum chemistry methods (John, 1988; Reichenbacher and Popp, 2012; Tunay Taşlı, 2022).

The structure of the title molecule is optimized by the DFT at B3LYP hybrid function that represents the Beckee-3-parameter, Lee-Yang-Parr with 6-311G (d,p) basis set, in the ground state (Becke, 1988; Becke, 1993; Mclean and Chandler, 1980). The bond length, bond angle, and dihedral angle as the structural properties obtained from the DFT calculation have been compared with the experimental data by linear regression analysis. The vibrational properties such as the Fourier Transform Infrared (FT-IR) spectra and some molecular vibrational behaviors have been investigated in the ground state by the DFT method with B3LYP/6-311G (d,p) basis set (Scott and Radon, 1996). The wavenumbers are found to be positive which indicates the success of the optimization process of the molecule. Each vibrational frequency has been analyzed via VEDA4 (Vibrational Energy Distribution Analysis) Program by using the Potential Energy Distribution (PED) (Jamroz and Dobrowolski, 2001; Jamroz, 2013). Because the DFT method overestimates the vibrational modes, the vibrational frequencies should be multiplied by the scaling factor of 0.966 for the used basic set (Jamroz, 2013). The UV-Vis absorption spectra have been revealed by utilizing the time-dependent density functional theory (TD-DFT) with B3LYP/6-311G (d,p) basis set (Ronca et al. 2014; The Beer-Lambert Law, 2022). ^{1}H and ^{13}C-NMR chemical shifts of the title

molecule have been predicted by employing GIAO method in the medium of DMSO (Scott and Radon, 1996; Wolinski et al., 1998).

The lowest unoccupied energy and the highest occupied energy of the orbitals (LUMO-HOMO energy) are computed by utilizing DFT/B3LYP/6-311G (d,p). Furthermore, the bandgap energy (E_g) of the molecule can be calculated from the energy level difference between HOMO and LUMO. Moreover, according to the Koopman's theorem (Sastri and Perumareddi, 1997), the energies of HOMO (E_{HOMO}) and LUMO (E_{LUMO}) have a relation with the ionization potential energy (IP), electron affinity (EA), electronegativity (x) (Pearson, 1986; Reichenbacher and Popp, 2012), chemical hardness (η) (Kaya, 2015), and global electrophilicity index (ω) (Perez et al., 2007), respectively, by the following relations;

$$IP = -E_{HOMO}, \tag{1}$$

$$EA = -E_{LUMO}, \tag{2}$$

$$x = \frac{1+EA}{2}, \tag{3}$$

$$\eta = \frac{1-EA}{2}, \tag{4}$$

and

$$\omega = \frac{x^2}{2\eta}. \tag{5}$$

3. Results and discussion

3.1. Optimized structure

The optimized structure shown in the Figure 1(b) has total 40 atoms (21 carbon, 16 hydrogen, 2 nitrogen, and 1 oxygen) and own 114 fundamental vibrational modes. The structural parameters such as bond length, bond angle, and dihedral angle are given in the Table 1, along with the comparison with the corresponding experimental results. The title molecule has 43 bond lengths, 69 bond angles and 50 dihedral angles.

Table 1. The optimized geometrical parameters via DFT/B3LYP/6-311G (d,p) and the corresponding experimental values (Crochet et al., 2011) of the molecule: the bond length data (Å) bond angles data (°) and dihedral angles (°).

No	Atom Labels	Bond Length (Å)	
		DFT	Exp
1	C1-C2	1.3996	1.3790
2	C1-C10	1.4038	1.3890
3	C1-N38	1.4151	1.4350
4	C2-H3	1.0835	0.9500
5	C2-C4	1.3910	1.3940
6	C4-H5	1.0841	0.9500
7	C4-C6	1.3932	1.3730
8	C6-H7	1.0842	0.9500

9	C6-C8	1.3980	1.3780
10	C8-H9	1.0845	0.9500
11	C8-C10	1.3874	1.3860
12	C10-H11	1.0816	0.9500
13	C12-C13	1.4445	1.4430
14	C12-C32	1.3780	1.3560
15	C12-N39	1.4073	1.4200
16	C13-C14	1.3960	1.3910
17	C13-C28	1.4411	1.4410
18	C14-H15	1.0820	0.9500
19	C14-C16	1.3997	1.3990
20	C16-C17	1.4281	1.4230
21	C16-C25	1.4397	1.4370
22	C17-H18	1.0849	0.9500
23	C17-C19	1.3672	1.3580
24	C19-H20	1.0843	0.9500
25	C19-C21	1.4240	1.4160
26	C21-H22	1.0842	0.9500
27	C21-C23	1.3670	1.3580
28	C23-H24	1.0850	0.9500
29	C23-C25	1.4278	1.4150
30	C25-C26	1.3985	1.3980
31	C26-H27	1.0825	0.9500
32	C26-C28	1.3959	1.3930
33	C28-C29	1.4397	1.4330
34	C29-C30	1.3787	1.3720
35	C29-O40	1.3544	1.3590
36	C30-H31	1.0812	0.9500
37	C30-C32	1.4089	1.4090
38	C32-H33	1.0822	0.9500
39	C34-H35	1.0948	0.9800
40	C34-H36	1.0883	0.9800
41	C34-H37	1.0948	0.9800
42	C34-O40	1.4234	1.4240
43	N38-N39	1.2576	1.2640

No	**Atom Labels**	**Bond Angle (Å)**	
		DFT	**Exp**
1	C2-C1-C10	119.5623	120.0
2	C2-C1-N38	115.4968	115.7
3	C10-C1-N38	124.9369	124.3
4	C1-C2-H3	118.1099	120.0
5	C1-C2-C4	120.3942	120.0
6	H3-C2-C4	121.4955	120.0
7	C2-C4-H5	119.9337	120.1
8	C2-C4-C6	119.9048	119.9
9	H5-C4-C6	120.1613	120.1
10	C4-C6-H7	120.1263	119.9
11	C4-C6-C8	119.8775	120.2
12	H7-C6-C8	119.9955	119.9
13	C6-C8-H9	119.7988	119.8
14	C6-C8-C10	120.4917	120.3
15	H9-C8-C10	119.7092	119.8
16	C1-C10-C8	119.7664	119.6
17	C1-C10-H11	118.9209	120.2
18	C8-C10-H11	121.3113	120.2
19	C13-C12-C32	119.5764	120.1
20	C13-C12-C39	116.6355	114.6
21	C32-C12-N39	123.7780	125.3
22	C12-C13-C14	122.6405	123.2
23	C12-C13-C28	118.8308	117.9
24	C14-C13-C28	118.5280	118.8
25	C13-C14-H15	118.5107	119.2
26	C13-C14-C16	121.8734	121.7
27	H15-C14-C16	119.6159	119.2
28	C14-C16-C17	122.1120	122.4
29	C14-C16-C25	119.3505	119.5
30	C17-C16-C25	118.5374	118.1
31	C16-C17-H18	118.5419	119.5
32	C16-C17-C19	120.9014	121.0
33	H18-C17-C19	120.5567	119.5
34	C17-C19-H20	120.1256	119.7
35	C17-C19-C21	120.5210	120.5
36	H20-C19-C21	119.3534	119.7
37	C19-C21-H22	119.4085	119.7
38	C19-C21-C23	120.3885	120.6
39	H22-C21-C23	120.2030	119.7
40	C21-C23-H24	120.5900	119.7
41	C21-C23-C25	120.8507	120.7
42	H24-C23-C25	118.5594	119.7
43	C16-C25-C23	118.8010	119.2
44	C16-C25-C26	118.9498	118.6
45	C23-C25-C26	122.2492	122.2
46	C25-C26-H27	119.5823	119.1

47	C25-C26-C28	121.4454	121.8
48	H27-C26-C28	118.9723	119.1
49	C13-C28-C26	119.8527	119.4
50	C13-C28-C29	118.8398	118.9
51	C26-C28-C29	121.3075	121.6
52	C28-C29-C30	120.5831	121.0
53	C28-C29-O40	114.8844	113.4
54	C30-C29-O40	124.5324	125.5
55	C29-C30-H31	120.9297	120.4
56	C29-C30-C32	120.2158	119.3
57	H31-C30-C32	118.8538	120.4
58	C12-C32-C30	121.9540	122.5
59	C12-C32-H33	118.1524	118.7
60	C30-C32-H33	119.8930	118.7
61	H35-C34-H36	109.4805	109.5
62	H35-C34-H37	109.5693	109.5
63	H35-C34-O40	111.2363	109.5
64	H36-C34-H37	109.4933	109.5
65	H36-C34-O40	105.7472	109.5
66	H37-C34-O40	111.2316	109.5
67	C1-N38-N39	115.3473	112.6
68	C12-N39-N38	115.7639	115.1
69	C29-O40-C34	118.9087	117.5

No	**Atom Labels**	**Dihedral Angle (°)**	
		DFT	**Exp**
1	C10-C1-C2-C4	0.6776	1.300
2	N38-C1-C2-C4	179.99	178.4
3	C2-C1-C10-C8	0.4449	1.600
4	N38-C1-C10-C8	179.69	178.2
5	C2-C1-N38-N39	173.30	173.3
6	C10-C1-N38-N39	7.4310	6.500
7	C1-C2-C4-C6	0.4445	0000
8	C2-C4-C6-C8	0.0219	1.100
9	C4-C6-C8-C10	0.2528	0.900
10	C6-C8-C10-C1	0.0170	0.500
11	C32-C12-C13-C14	179.88	175.80
12	C32-C12-C13-C28	0.2082	5.100
13	N39-C12-C13-C14	1.2309	3.000
14	N39-C12-C13-C28	179.10	176.1
15	C13-C12-C32-C30	0.1290	2.600
16	N39-C12-C32-C30	178.93	178.8
17	C13-C12-N39-N38	173.26	167.4
18	C32-C12-N39-N38	7.9029	13.90
19	C12-C13-C14-C16	179.87	178.8
20	C28-C13-C14-C16	0.1977	0.300
21	C12-C13-C28-C26	179.84	176.7
22	C12-C13-C28-C29	0.1426	3.900
23	C14-C13-C28-C26	0.1584	2.400
24	C14-C13-C28-C29	179.82	177.0
25	C13-C14-C16-C17	179.92	179.3
26	C13-C14-C16-C25	0.1130	1.700
27	C14-C16-C17-C19	179.99	180.0
28	C25-C16-C17-C19	0.0364	1.000
29	C14-C16-C25-C23	179.99	179.7
30	C14-C16-C25-C26	0.0141	1.700
31	C17-C16-C25-C23	0.0296	0.700
32	C17-C16-C25-C26	179.95	179.3
33	C16-C17-C19-C21	0.0177	0.900
34	C17-C19-C21-C23	0.0084	0.600
35	C19-C21-C23-C25	0.0147	0.400
36	C21-C23-C25-C16	0.0046	0.400
37	C21-C23-C25-C26	179.97	179.0
38	C16-C25-C26-C28	0.0501	0.400
39	C23-C25-C26-C28	179.97	178.1
40	C25-C26-C28-C13	0.0364	2.500
41	C25-C26-C28-C29	179.95	176.9
42	C13-C28-C29-C30	0.0035	0000
43	C13-C28-C29-O40	179.84	178.4
44	C26-C28-C29-C30	179.99	179.4
45	C26-C28-C29-O40	0.1671	1.000
46	C28-C29-C30-C32	0.0876	2.700
47	C28-C29-O40-C34	179.80	179.5
48	C30-C29-O40-C34	0.3618	2.200
49	C29-C30-C32-C12	0.0208	1.500
50	C1-N38-N39-C12	178.22	179.6

In addition, to get the proper correlation between the experimental and calculation result, linear regression analysis is considered. The linear regression is provided by the linear equation of $y = ax + b$, where a and b are the fit parameters. The results are presented in Figure 2. The regression values of bond length, bond angle, and dihedral angle are calculated as 0.99516, 0.92783 and 0.99967, respectively, which indicates that they have a good agreement between the calculation and experimental results and verify that the DFT method produces the compatible data for the title molecule (Cameron and Windmeijer, 1995; Kohn and Sham 1965).

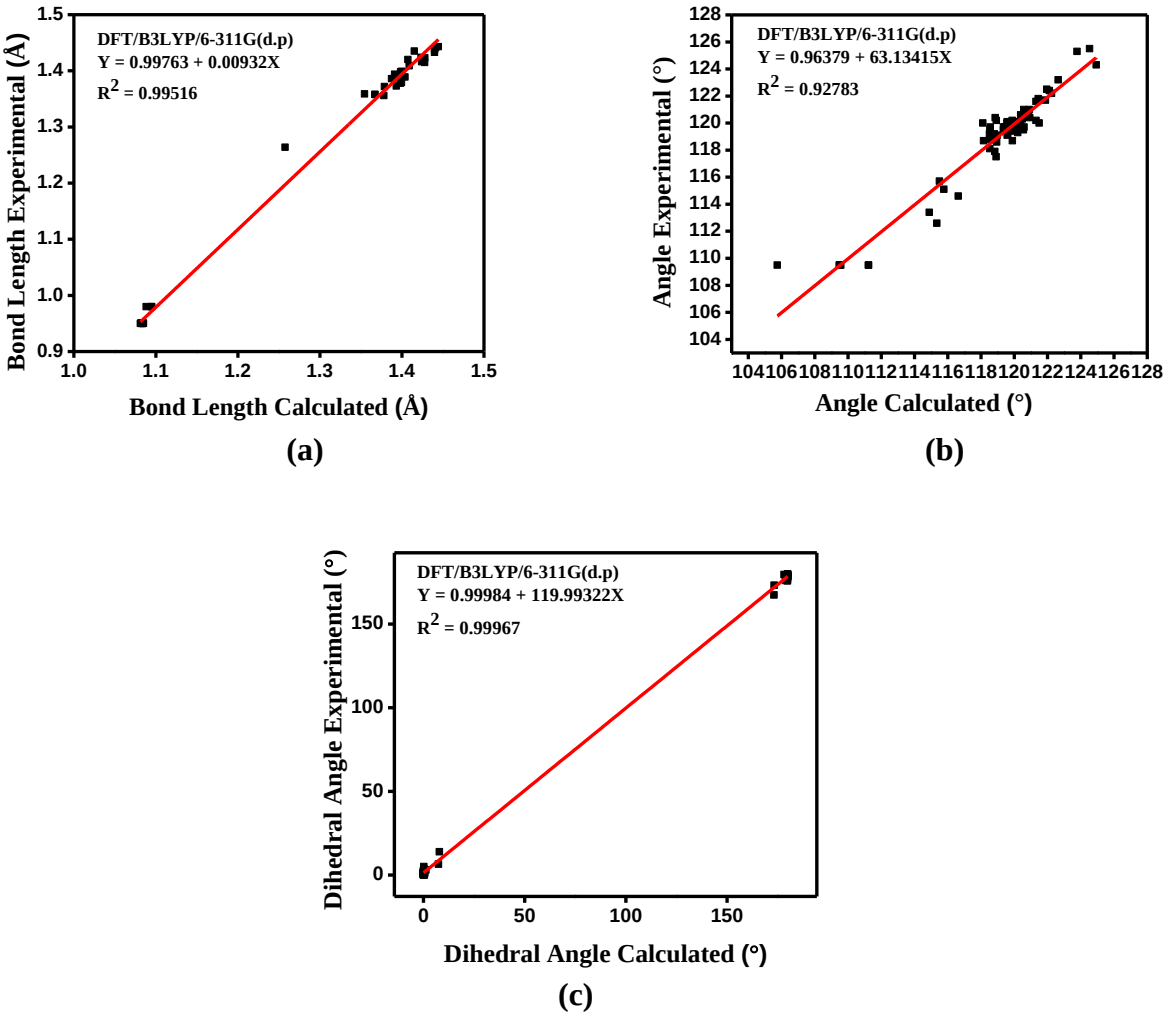

Figure 2. Linear regression between the DFT and experimental values of **(a)** bond lengths (Å), **(b)** bond angles (°) and **(c)** dihedral angles (°).

3.2. FT-IR and vibrational modes

Infrared spectroscopy (IR) shows important information about the nature of the chemical and molecular bond and intramolecular forces acting between the atoms and intermolecular forces in a condensed phase. A molecule can vibrate in many ways, called a vibrational mode (Spectroscopy Data Tables: Infrared Tables). Generally, the simulated FT-IR spectra are used to determine the molecular structure and identify the chemical compounds, and states of the title molecules. The title molecule has 40 (N) atoms with 114 $((3 \times N) - 6)$ fundamental vibrational modes. The FT-IR spectra are depicted in Figure 3. The basic vibrational modes such as stretching, bending and torsion modes are analyzed as: Of these 114 basic vibration modes, 39 $(N - 1)$ as stretching modes, 38 $(N - 2)$ as bending modes, and 37 $(N - 3)$ as torsion modes (Jamroz and Dobrowolski, 2001).

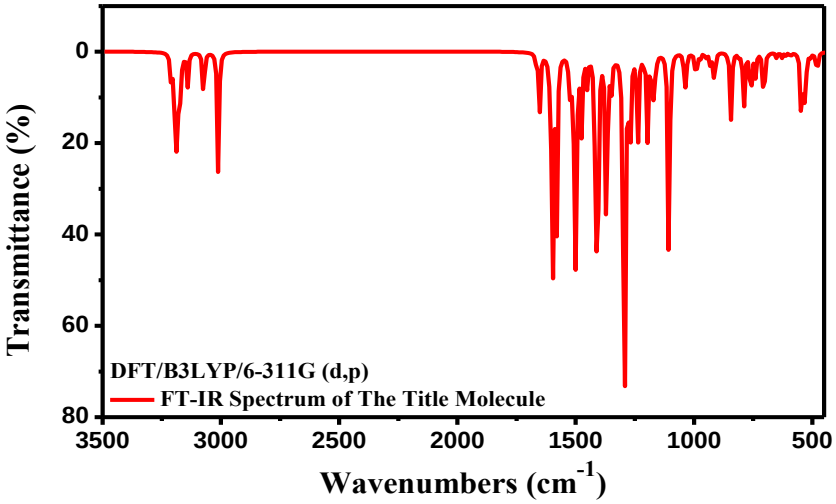

Figure 3. The FT-IR spectrum of the title molecule by using DFT method.

The normal mode assignments of the vibrational frequencies of the title molecule are listed in Table 2. Based on the spectroscopy data in the literature (Spectroscopy Data Tables: Infrared Tables), the peaks from 3100 – 3000 cm^{-1} indicates an unsaturated system (alkenes, sp^2), while the range from 3000 – 2850 cm^{-1} belongs to saturated systems (alkanes, sp^3) of carbon hydrogen atoms. The carbon and carbon atoms show at about 1700 – 1500 cm^{-1} or the vibrational mixed modes at 1400 – 1300 cm^{-1}. Moreover, the azo group shows the stretching modes in the main region at about of 1600 – 1300 cm^{-1}. The chemical group of oxygen and carbon atoms presents the stretching modes at 1250 – 1000 cm^{-1}. As for interest in the results of the DFT simulation, the C-H stretching (ν CH) mode appears mostly between 3105.4 and 2911.86 cm^{-1}. The C-C stretching (ν CC) mode in an aromatic group shows in two peaks at the regions of 1598.58 – 1545.44 cm^{-1} and 1363 – 1324.3 cm^{-1}. The stretching modes (ν NN) of the azo compound of the title molecule present in a single peak at 1424.8 cm^{-1}, while the stretching mode between oxygen and carbon (ν OC) exhibits at 1253.3 and 1069.9 cm^{-1}.

Table 2. The vibrational wavenumbers (cm^{-1}) of the title molecule by DFT/B3LYP/6-311G (d,p), IR intensities ($km.mol^{-1}$), and assignment with PED percentage in the square brackets. Scaled factor is taken as 0.967 for DFT/6-311G (d,p).

Mode	DFT/B3LYP /6-311G (d,p)		I^{IR}	Assignment [PED]>10%
	Unscaled	Scaled		
1	16.800	16.260	0.0703	τ NNCC (41) + τ CCNN (44)
2	40.490	39.150	0.9518	τ CCCC (11) + τ CCNN (12) + τ CNNC (30) + γ CCNC (14) + γ NCCC (10)
3	48.140	46.550	0.5250	δ NNC (29) + δ CCN (11) + δ CNN (31)
4	69.800	67.500	2.2645	τ CCCN (21) + τ CCCC (15) + τ COCC (24)
5	84.360	81.580	0.5143	τ NNCC (18) + τ CCCC (43)
6	94.950	91.820	1.0294	τ NNCC (11) + τ CCCC (31)
7	126.06	121.90	2.0733	τ COCC (51)
8	146.72	141.88	4.9566	δ CCC (24) + δ OCC (19)
9	168.66	163.09	1.2546	δ NCC (11)

10	184.40	178.31	0.7803	δ NCC (11)
11	230.82	223.20	0.3843	ν NC (11)
12	240.98	233.03	0.2865	τ HCOC (71)
13	256.11	247.66	0.3121	τ CCCC (48) + τ CCCN (10)
14	258.84	250.29	0.9493	τ CCCC (19) + γ CCNC (16) + γ NCCC (11)
15	291.34	281.73	0.6335	τ CCCC (17) + τ CNNC (13)
16	312.41	302.10	0.4532	δ CCC (20) + δ COC (10)
17	333.91	322.89	1.7371	δ COC (40)
18	387.13	374.35	9.3841	δ NCC (11)
19	404.95	391.59	1.1214	τ CCCC (28) + γ OCCC (12)
20	414.94	401.25	0.7535	τ CCCC (36)
21	420.87	406.98	0.1745	τ HCCC (11) + τ CCCC (75)
22	479.63	463.80	15.133	τ HCCC (20) + τ CCCC (37) + γ CCCC (15)
23	487.40	471.32	1.4298	δ CCC (18)
24	507.27	490.53	2.2282	τ CCCC (25)
26	536.15	518.46	18.117	γ NCCC (12)
27	545.87	527.86	43.881	δ CCC (14) + δ COC (15)
28	591.68	572.15	2.8111	δ CCC (11) + δ CCN (11)
29	613.09	592.86	2.0135	τ CCCC (26)
30	628.12	607.39	3.2926	δ CCC (40)
31	631.21	610.38	0.2164	δ CCC (56)
32	651.18	629.69	2.5174	τ CCCN (13) + τ CCCC (11) + γ OCCC (24)
34	681.79	659.29	0.4352	δ CCC (17) + δ CCC (10)
35	704.35	681.11	39.692	τ HCCC (61) + τ CCCC (27)
37	759.56	734.49	34.911	τ HCCC (50) + ν CC (30)
38	769.05	743.67	0.9850	τ HCCC (13) + γ CCCC (16)
39	788.24	762.23	22.091	τ HCCC (23)
41	807.48	780.83	0.0077	τ HCCC (12) + γ CCNC (11)
43	843.55	815.71	43.092	τ HCCC (75)
44	857.62	829.32	0.2722	τ HCCC (98)
45	859.73	831.36	0.6165	τ HCCC (66)
46	913.19	883.06	22.964	τ HCCC (51) + τ CCCC (19)
47	924.07	893.58	1.7713	δ CCC (14)
48	929.04	898.38	1.6248	δ CNN (10) + τ HCCC (15)
49	932.52	901.75	6.3059	τ HCCC (48)
50	950.78	919.40	4.1912	τ HCCC (71)
51	972.37	940.28	3.2561	τ HCCC (80)
52	982.21	949.80	1.8000	τ HCCC (64) + τ CCCC (17)
53	992.15	959.41	19.470	τ HCCC (41) + δ CCC (14)
54	992.58	959.82	0.2763	τ HCCC (73)
55	997.07	964.17	0.0156	τ HCCC (90)
56	1007.6	974.35	0.4396	τ HCCC (47) + τ CCCC (39)
57	1014.6	981.10	0.1562	ν CC (11) + δ CCC (64)
58	1029.0	995.05	3.8318	ν CC (51)

59	1037.9	1003.6	25.136	ν NC (10)
60	1042.2	1007.8	1.4669	ν CC (15) + ν NC (10)
61	1097.4	1061.2	4.4833	ν CC (28) + δ HCC (44)
62	1106.5	1069.9	143.04	ν CC (12) + ν OC (25) + δ HCC (10)
63	1155.7	1117.6	2.4389	ν NC (10) + δ HCC (10)
64	1168.9	1130.3	29.641	ν CC (10) + δ HCC (26)
65	1170.3	1131.6	0.8262	δ HCH (31) + τ HCOC (69)
66	1173.5	1134.7	6.4095	δ HCC (12)
67	1178.0	1139.2	10.281	δ HCC (42)
68	1179.8	1140.8	0.6157	ν CC (11) + δ HCC (67)
69	1196.1	1156.6	54.623	δ HCC (10)
70	1214.3	1174.2	5.2411	δ HCC (13) + δ HCH (11) + τ HCOC (38)
71	1237.1	1196.3	57.674	ν CC (12) + ν OC (10)
72	1243.7	1202.7	1.4759	ν NC (24)
73	1270.9	1229.0	75.915	ν NC (14) + δ HCC (25)
74	1292.2	1249.6	109.72	δ HCC (51)
75	1296.1	1253.3	200.04	ν CC (10) + ν OC (19) + δ HCC (13)
76	1333.7	1289.7	1.1130	ν CC (13) + δ HCC (60)
77	1347.2	1302.7	6.2969	ν CC (25)
79	1369.5	1324.3	135.55	ν CC (40)
80	1405.7	1359.3	67.014	ν CC (10) + δ CCC (11)
81	1409.8	1363.3	115.59	ν CC (14)
82	1417.8	1371.0	48.361	δ HCC (12)
84	1473.4	1424.8	8.7626	ν NN (13)
85	1476.6	1427.9	43.065	δ HCH (31)
86	1491.9	1442.6	3.4471	δ HCH (10)
87	1491.9	1442.6	8.9335	δ HCH (77) + τ HCOC (15)
88	1501.8	1452.3	158.39	δ HCH (46)
89	1507.1	1457.3	1.8763	δ HCH (27)
90	1513.2	1463.3	15.58	δ HCC (22) + δ HCH (12)
91	1525.7	1475.3	25.36	ν NN (32) + δ HCC (14)
93	1598.2	1545.44	175.84	ν CC (10)
94	1611.2	1558.02	6.3083	ν CC (33)
95	1623.5	1569.91	1.3237	ν CC (44) + δ CCC (11)
96	1640.3	1586.16	1.1052	ν CC (56)
97	1653.1	1598.58	39.283	ν CC (53)
98	1668.3	1613.28	4.7266	ν CC (50)
99	3011.2	2911.86	78.748	ν CH (91)
100	3073.3	2971.87	33.744	ν CH (100)
101	3140.0	3036.39	21.060	ν CH (91)
102	3158.1	3053.92	1.0756	ν CH (100)
103	3162.3	3057.98	2.7320	ν CH (97)
104	3163.7	3059.30	0.4524	ν CH (95)
105	3172.3	3067.6	12.041	ν CH (87)

106	3176.0	3071.2	27.824	ν CH (99)
107	3184.4	3079.3	27.739	ν CH (91)
108	3187.7	3082.5	35.703	ν CH (90)
109	3194.3	3088.9	22.752	ν CH (97)
110	3197.9	3092.5	2.590	ν CH (94)
111	3199.2	3093.6	10.590	ν CH (96)
112	3204.1	3098.4	1.1902	ν CH (97)
113	3211.0	3105.1	3.7544	ν CH (95)
114	3211.4	3105.4	11.567	ν CH (99)

a) PED: potential energy distribution. ν; stretching, δ; in-plane-bending, γ; out-of-plane bending, τ; torsion.

3.3. ^{1}H and ^{13}C-NMR spectra

The characteristic of chemical shifts, obtained from magic-angle spinning NMR (Nuclear Magnetic Resonance) spectra, provide valuable information on the crystallography or structure of the molecules (Claramunt et al., 2006; Harris, 2004). The types of the spectra observed depend on the activation energy identifying the tautomer group (determining the lifetimes of the states) and the variation in the chemical shift. The results are given in Table 3.

Table 3. The chemical shifts of the ^{1}H and ^{13}C-NMR in the medium of DMSO solvent by employing DFT/B3LYP/6-311G (d,p) (all values in ppm).

^{13}C-NMR		**^{1}H-NMR**	
Atomic Symbol	DFT/B3LYP/6-311G (d,p)	**Atomic Symbol**	DFT/B3LYP/6-311G (d,p)
C29	167.1392	**H15**	10.001
C1	157.2794	**H27**	9.2718
C12	144.3755	**H11**	8.4099
C2	137.5361	**H33**	8.4098
C16	136.3036	**H18**	8.4097
C6	135.5350	**H24**	8.4068
C13	135.5037	**H3**	8.3398
C25	134.5380	**H5**	7.8861
C4	133.4310	**H20**	7.8643
C23	133.3690	**H22**	7.8182
C8	132.9520	**H9**	7.7848
C17	132.7623	**H7**	7.7089
C19	131.1299	**H31**	6.9611
C21	130.0430	**H36**	4.5001
C28	127.9057	**H35**	4.0718
C26	126.0042	**H37**	4.0620
C14	125.1764		
C10	116.0638		
C32	114.5191		
C30	104.1893		

C34	55.90290

The labels of the atoms in this table are given according to Figure 1 (b).

The chemical shifts of ^{13}C-NMR are presented between 167.14 ppm – 55.90 ppm. The carbon aromatic group appears between 167.14 – 104.19 ppm, as seen in Table 3. On the other hand, those of ^{1}H-NMR are predicted as 10 – 4 ppm. The hydrogen aromatic ring (Ar – H) exists in the interval of 10 – 6.96 ppm.

3.4. Absorbance spectrum

Ultraviolet-Visible (UV-Vis) absorption spectroscopy is the measurement of a beam reduction after being reflected from a sample surface or passed through a sample. It is also associated with the resonating structures in the molecules. The UV-Vis quantitative determination is based on the Beer-Lambert law, which is generally used in any solvent (Behera et al., 2014; The Beer-Lambert Law, 2022). It can be reported from Figure 4 that the maximum absorption peak appears at 506.33 nm in the visible region (blue).

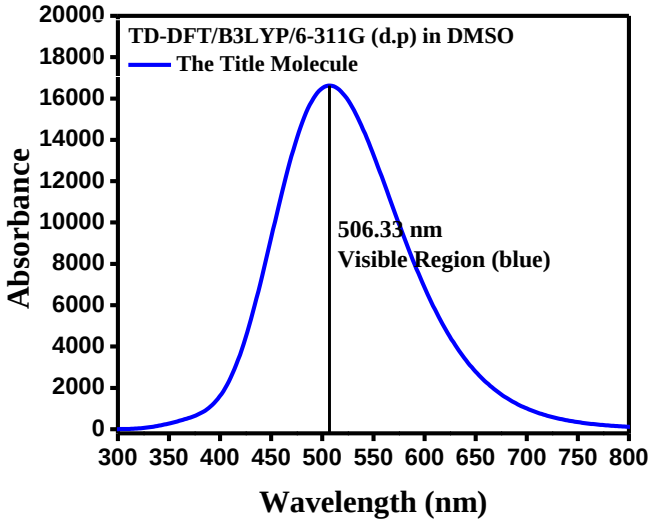

Figure 4. The absorbance spectrum of the title molecule in the excited state by using TD-DFT method.

3.5. Electronic properties

The electronic properties of the title molecule can be analyzed by utilizing HOMO-LUMO energy interactions. The HOMO-LUMO energy levels are shown in Figure 5 and the values of the electronic properties of the molecule considered in this study are collected in Table 4.

The bandgap energy is found as 2.85 eV which represents that the molecule shows a semiconductor behavior. The ionization potential energy is associated with the amount of required energy to remove an electron from an isolated atom or the capability of a molecule to enter chemical reactions. It is predicted as about 5.28 eV (low IP). The electron affinity (EA) of the title molecule indicating the amount of energy when an electron is added to a neutral atom to form a negatively charged ion is calculated as 2.43 eV. The electronegativity (x) is obtained as 3.86 eV (near Fluorine), which gives the ability of the polarization of the title molecule. The chemical

hardness and the global electrophilicity index of the title molecule are evaluated as 1.42 eV (low η) and 5.21 eV, respectively (John, 1988).

Table 4. The electronic properties (all values in eV) of the title molecule.

	Electronic Properties
E_{LUMO}	-2.43
E_{HOMO}	-5.28
E_g	2.85
IP	5.28
EA	2.43
x	3.86
η	1.43
ω	5.21

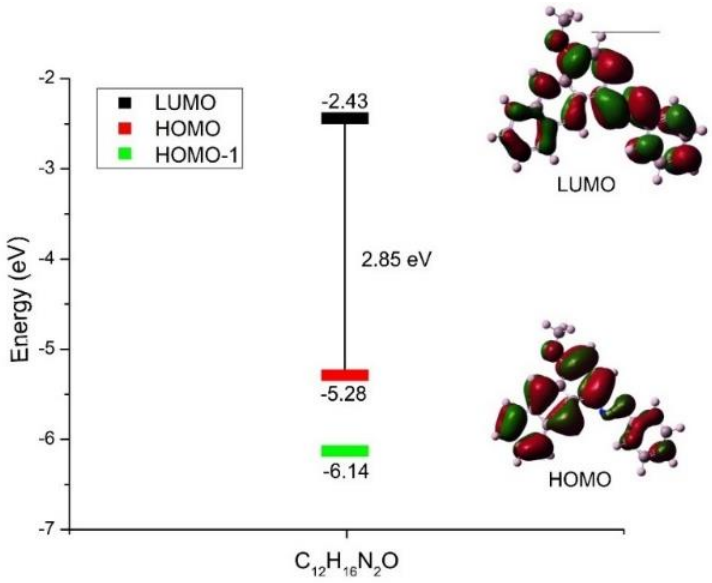

Figure 5. The HOMO-LUMO levels of the title molecule.

4. Conclusion

The characterization of the title molecule is conducted theoretically for the first time in this study. The structural properties are computed by the DFT method such as bond length, bond angle and dihedral angle are in excellent agreement with those observed. The FT-IR spectra show that the title molecule has 114 vibrational modes specified with the stretching, in-plane-bending, out-of-plane-bending, and torsion vibrations. The chemical shifts of the ^{1}H and ^{13}C-NMR for the aromatic groups in the medium of DMSO solvent are identified. The UV-Vis spectra show that the molecule absorbs energy in the visible region. The HOMO-LUMO energy level represents that the molecule displays a semiconductor character. As a result, in this study, the structural and spectroscopic properties of the title molecule whose only structural properties have been measured (Crochet et al., 2011) are evaluated by the ab-initio calculations to provide a complete understanding of the molecule behavior. The results computed in this study are expected to be valuable information for future experiments and research.

Acknowledgements

This study has been supported by Pamukkale University (Grant No: BAP-2021FEBE063).

Conflict of interest

All authors state that there is no conflict of interest.

CRediT Author Statement

Author 1 (AQA): Formal analysis, Investigation, Data Curation, Writing - Original Draft.

Author 2 (PTT): Conceptualization, Methodology, Validation.

Author 3 (SOK): Conceptualization, Methodology, Validation, Resources, Project Administration, Supervision, Writing – Review & Editing.

References

Alsantali R.I., Raja Q.A., Alzahrani A.Y.A., Sadiq A., Naeem N., Mughal E.U., Al-Rooqi M.M., Guesmi N.E., Moussa Z., Ahmed S.A., 2022. Miscellaneous azo dyes: a comprehensive review on recent advancements in biological and industrial applications. Dyes and Pigments, 199:110050.

Balci M., 2005. Basic ^{1}H- and ^{13}C-NMR Spectroscop, 1st. Elsevier Science, Ankara. 25 – 85 p.

Bauernschmitt R., Ahlrichs R., 1996. Treatment of electronic excitations within the adiabatic approximation of time dependent density functional theory. Chemical Physics Letter, 256(4-5):454-464.

Bayer E.B., Rochester N.Y., 1976. Color Imaging Array. United States Patent, United States. 350 – 317 p.

Becke A.D., 1988. Density-functional exchange-energy approximation with correct asymptotic behavior. APS Physical Review A, 38(6): 3098–3100.

Becke A.D., 1993. Density functional thermochemistry. III. The role of exact exchange. Journal of Chemical Physics, 7(98):5648-5652.

Becker E.D., 2000. High Resolution NMR Theory and Chemical Applications, 3rd. Academic Press, U.S.A. 83-177 p.

Behera P.K., Xess A., Sahu S., 2014. Solvent Effect on the Electronic Spectra of Some Heterocyclic Azo Dyes. Bulletin of The Korean Chemical Society, 35(2):610- 616.

Benkhaya S., M'rabet S., El Harfi A., 2020. Classifications, properties, recent synthesis and applications of azo dyes. Heliyon, 6(1):e03271.

Cameron A.C., Windmeijer F.A.G., 1997. An R-squared measure of goodness of fit for some common nonlinear regression models. Journal of Econometrics. 77(2):329-342.

Claramunt R.M., Lopez C., Maria D.S., Sanz D., Elguero J., 2006. The use of NMR spectroscopy to study tautomerism. Progress in Nuclear Magnetic Resonance Spectroscopy, 49(3-4):169-206.

Crochet A., Fromm K.M., Kurteva V., Antonov L., 2011. (E)-1-(4-Methoxyanthracen-1-yl)-2-phenyldiazene. Acta Crystallographica Section E-Structure Reports Online, 67:1600-5368.

Coelho P.J., Castro C.R., Fernandes S.S.M., Forcensa A.M.C., Raposo M.M.M., 2012. Enhancement of the photochromic switching speed of bithiophene azo dyes. Tetrahedron Letters, 53(34): 4502 – 4506.

Chen X.C., Tao T., Wang Y.G., Peng Y.X., Huang W., Qian H.F., 2012. Azo-hydrazone tautomerism observed from UV-Vis spectra by pH control and metal-ion complexation for two heterocyclic disperse yellow dyes. Dalton Transactions, 41(36): 11107–11115.

Frisch, M. J. 2016. Gaussian 09. Available from: https://gaussian.com/g09citation/

Habibi M.H., Hassanzadeh A., Isfahani A.Z., 2006. Effect of dye aggregation and azo-hydrazone tautomerism on the photocatalytic degradation of Solophenyl red 3BL azo dye using aqueous TIO_2 suspension. Dyes and Pigments, 69(3):111-117.

Harris R.K., 2004. NMR crystallography: the use of chemical shifts. Solid State Sciences, 6(10):1025-1037.

Huang Y., Yr Q., Li., Zheng M., Yan B., et al., 2022. Preparation of a redox mediator membrane and its application to catalyzing biodegradation of azo dyes. Journal of Environmental Chemical Engineering, 10(3): 107778.

Jamroz M.H., Dobrowolski J.Cz., 2001. Potential energy distribution (PED) analysis of DFT calculated IR spectra of the most stable Li, Na, and Cu(I) diformate molecules. Journal of Molecular Structure, 565: 475 – 480.

Jamroz M.H., 2013. Vibrational Energy Distribution Analysis (VEDA): Scopes and limitations. Spectrochimica Acta Part A-Molecular and Biomolecular Spectroscopy, 114: 220 – 230.

John E., 1988. The Elements 3, 3rd. Oxford Clarendon Press, New York.

Karabacak Atay Ç., Ozdemir Kart S., Gökalp M., Tuğrul Ö., Tilki T., 2019. Characterization and absorption properties of newly synthesized mono azodyes: Experimental and theoretical approach. Journal of Molecular Structure, 1180:251-259.

Kaya S., Kaya C., 2015. A New Method for Calculation of Molecular Hardness: A Theoretical Study. Computational and Theoretical Chemistry, 1060:66-70.

Kelemen J., 1981. Azo-hydrazone tautomerism in azodyes. I. A comparative study of 1-phenylazo-2-naphthol and 1-phenylazo-2-naphthylamine derivatives by electronic spectroscopy. Dyes and Pigments, 2(2):73–91.

Kohn W., Sham L.J., 1965. Self-Consistent Equations Including Exchange and Correlation Effects. Physical Review Journals Archive, 140: A1133.

Lee H.Y., Song X., Park H., Baik M.H., Lee D., 2010. Torsionally Responsive C_3-Symmetric Azodyes: Azo-Hydrazone Tautomerism, Conformational Switching, and Application for Chemical Sensing. Journal of The American Chemical Society, 132(34): 12133-12144.

Lee T.D., Yang C.N., 1959. Many-Body Problem in Quantum Statistical Mechanics. I. General Formulation. Physical Review Journal Archive, 113: 1165.

McLean A.D., Chandler G.S., 1980. Contracted Gaussian basis set for molecular calculations. I. Second row atoms, Z=11-18. AIP The Journal of Chemical Physics, 72: 5639.

Pearson R.G., 1986. Absolute electronegativity and hardness correlated with molecular orbital theory. Proceedings of the National Academy of Sciences of The United States of America, 83(22):8440-8441.

Pearson R.G., 1997. Chemical Hardness. John Wiley-VCH, Weinheim, 175 – 195p.

Perez P., Domingo L.R., Aizman A., Contreras R., 2007. The Electrophilicity index in organic chemistry. Theoretical and Computational Chemistry, 19:139-201.

Reichenbacher M., Popp J., 2012. Challenges in Molecular Structure Determination. Springer-Verlag Berlin Heidelberg, 63-143 p.

Ronca E., Angeli C., Belpassi L., De Angelis F., Tarantelli F., Pastore M., 2014. Density relaxation in Time-Dependent Functional Theory: Combining Relaxed Density Natural Orbitals and Multireference Perturbation Theories for an Improved Description of Excited States. Journal of Chemical Theory and Computation, 10(9):4014-4024.

Rong C.Y., Wang B., Zhao D.B., Liu S.B., 2019. Information-theoretic approach in density functional theory and its recent applications to chemical problems. Wiley Interdiciplinary Reviews-Computational Molecular Science, 10(4):e1461.

Sastri V.S., Perumareddi J.R., 1997. Molecular Orbital Theoretical Studies of Some Organic Corrosion Inhibitors. Corrosion, 53(8):671-622.

Scott A.P., Radon L., 1996. Harmonic Vibrational Frequencies: An Evaluation of Hartree−Fock, Møller−Plesset, Quadratic Configuration Interaction, Density Functional Theory, and Semiempirical Scale Factors. Journal of Physical Chemistry, 100(41): 16502-16513.

Shawali A.L., Abdallah M.A., Mosselhi M.A.N., Elhorbany Y.F., 2002. Synthesis and tautomeric structure of 1,2-bis-(7-arylhydrazono-7H-[1,2,4]triazolo[3,4-b][1,3,4]thiadiazin-3-yl) ethanes. Zeitschrift Fur Naturforschung Section B-A Journal of Chemical Sciences, 57(5):552–556.

Spectroscopy Data Tables: Infrared Tables. Available from: https://www.cpp.edu/~psbeauchamp/pdf/spec_ir_nmr_spectra_tables.pdf

The Beer-Lambert Law. 2022. Available from: https://www.edinst.com/blog/the-beer-lambert-law/#:~:text=The%20Beer%2DLambert%20law%20states,calculated%20by%20measuring%20its%20absorbance.

Tunay Taşlı P., Karabacak Atay Ç., Demirturk.T., Tilki T., 2020. Experimental and computational studied of newly synthesized azo dyes based materials. Journal of Molecular Structure, 1201: 127098.

Wolinski K., Haacke R., Hinton J.F., Pulay P., 1998. Methods for parallel computation of SCF NMR chemical shifts by GIAO method: Efficient integral calculation, multi-Fock algorithm, and pseudodiagonalization, Journal of Computational Chemistry, 18(6): 816–825.

Yıldırım F., Demirçalı A., Tunay Taşlı P., Karcı F., 2021. New disazodyes derived from aminopyrazoles: synthesis, spectroscopic properties, computational study and structural properties. Coloration Technology, 137(4): 336-347.